REPORT DOCUMENTATION PAGE

Public reporting burden for this collection of information is estimated to average 1 hour per response, including the time for reviewing instructions, searching existing data sources, gathering and maintaining the data needed, and completing and reviewing the collection of information. Send comments regarding this burden estimate or any other aspect of this collection of information, including suggestions for reducing this burden, to Washington Headquarters Services, Directorate for Information Operations and Reports, 1215 Jefferson Davis Highway, Suite 1204, Arlington, VA 22202-4302, and to the Office of Management and Budget, Paperwork Reduction Project (0704-0188), Washington, DC 20503.

1. AGENCY USE ONLY (Leave blank)	2. REPORT DATE	3. REPORT TYPE AND DATES COVERED
	Dec. 28, 1995	Final Tech 01/08/92 - 31/07/95

4. TITLE AND SUBTITLE

Regularization of Localized Degradation Processes

5. FUNDING NUMBERS

F49620-92-J-0442

AFOSR-TR.
97-0483

6. AUTHOR(S)

Willam, Kaspar J.

7. PERFORMING ORGANIZATION NAME(S) AND ADDRESS(ES)

CEAE-Department
University of Colorado Boulder
Boulder, CO 80309 - 0428

8. PERFORMING ORGANIZATION REPORT NUMBER

153-7208

9. SPONSORING/MONITORING AGENCY NAME(S) AND ADDRESS(ES)

Air Force Office of Scientific Research
Bolling Air Force Base
Washington, DC 20332-6448

NA

10. SPONSORING/MONITORING AGENCY REPORT NUMBER

11. SUPPLEMENTARY NOTES

Project Award F 49620-92-J-0442, Acct 1-5-37208

12a. DISTRIBUTION/AVAILABILITY STATEMENT

unrestricted   Approved for public release;
distribution unlimited.

12b. DISTRIBUTION CODE

13. ABSTRACT (Maximum 200 words)

Localization and the formation of spatial discontinuities indicate the onset of failure in materials which are subjected to degradation from a continuum into a discontinuum.
In this project explicit analytical and geometrical Mohr-type envelope methods were developed to determine discontinuous failure modes in elastoplastic softening and elastic damaging materials. These localization results were obtained for classical non-polar continua in order to assess the regularization properties of non-classical micropolar Cosserat continua which feature non-symmetric stress and strain tensors because of the presence of couple-stresses and micro-curvatures. It was shown that micropolar media may only exhibit localized failure in the form of tensile mode I, while shear failure appears only in a distributed form without forming discontinuities.

14. SUBJECT TERMS

Failure Mechanics, Localization Analysis, Softening and Elastic Damage, Regularization of Cosserat Continua, Spatial Discontinuities

15. NUMBER OF PAGES

16. PRICE CODE

17. SECURITY CLASSIFICATION OF REPORT	18. SECURITY CLASSIFICATION OF THIS PAGE	19. SECURITY CLASSIFICATION OF ABSTRACT	20. LIMITATION OF ABSTRACT
UNCLASSIFIED	UNCLASSIFIED	UNCLASSIFIED	UL

NSN 7540-01-280-5500

DTIC QUALITY INSPECTED 3

US-AFOSR Award F 49620-J-0442

"Regularization of Localized Degradation Processes"

Introductory Remarks

Deterioration science is a field of critical importance when the life-cycle behavior and the limit state performance of structures are to be assessed. In view of the widespread use of cohesive-frictional materials in construction, the degradation of stiffness, strength and ductility are of paramount importance. Mismatch of the constituent properties in heterogeneous media, and in cohesive particle composites in particular, leads to distributed deterioration in the form of damage due to randomly oriented microdefects. Mechanical overloading results in localized deterioration and the formation of macrodefects which are ultimately responsible for the collapse of structural components and structural systems.

Accomplishments

The main focus of this effort was to examine the regularization properties of Cosserat continua on the formation of weak discontinuities. In that context we were able to show analytically that localization in the form of discontinuous bifurcation is suppressed except for decohesive mode I type failure modes, when strain softening plasticity and scalar damage formulations were considered. Consequently, mixed mode and mode II type failure mechanisms remain continuous and do not exhibit spatial discontinuities unlike cassical non-polar continua. The main finding was however the geometric representation of non-symmetric stresses and strains in terms of generalized Mohr's circle which are characteristic for micropolar continua, see WILLAM ET AL, [1995A]. This led to a fundamental investigation of discontinuous failure where the localization limiter plots as an ellipse in the Mohr cooordinates WILLAM AND IORDACHE, [1994B]. This graphic approach was used to study distributed versus localized failure 'in the small' WILLAM AND IORDACHE, [1995B] selected results of which are shown in the next section. Results of the failure studies 'in the large' are presented in IORDACHE, [1995] for both homogeneous and heterogeneous media of two-phase particle composites. These observations demonstrate that the failure mode of the localization study in the small transpires also at the structural level (solution of the IBVP), and they illustrate the dramatic effect of softening on the overall ductility of the composite.

On the experimental side, new insight was obtained from uniaxial compression test when concrete specimens of different height LEE AND WILLAM, [1995A] were subjected to load-unload-reload cycles to separate elastic stiffness degradation (damage) from the degradation of strength (softening). A novel anisotropic hardening/softening formulation was developed for concrete LEE AND WILLAM, [1995B] using a generalization of vertex-type plasticity. Moreover, preliminary work was performed in the area of ultrasonic material characterization leading to a proof of concept to detect localized failure in steel specimens which were subjected to

plastic yielding, see RADAKOVIC ET AL. [1995].

Resources and Personnel:
The project did support one graduate PhD student and provided partial support for one undergraduate student and one part-time post-doctoral student aside from the PI. Two members of the team were US citizens, and two were women. In the course of the AFOSR award one PhD thesis is currently being completed, IORDACHE [1995].
For the sake of appreciation of failure analysis in the small, some of the findings WILLAM AND IORDACHE, [1994B], [1995B] are summarized below, omitting the added complexities of Cosserat continua which were discussed in WILLĀM ET AL, [1995A], and which are currently expanded by IORDACHE, [1995] in her thesis.

Failure Analysis in the Small:

There are three basic descriptors at our disposal to diagnose failure in the small, which lend themselves to the following classification WILLAM ET AL, [1994A]:
The failure indicators that characterize failure at the constitutive level may be classified according to the following concepts :

- Limit State Condition: $F = F(\sigma, \mathbf{q}) = 0$.
  The limit state condition is a generalization of the traditional maximum strength concept and delimits the triaxial state of stress σ according to the underlying failure hypothesis. This strength condition depends, in general, on the internal variables $\mathbf{q}$ which characterize the current state of the material. In the simplest case we recover the classic concept of the Mohr failure envelope which states that the state of normal and tangential tractions on the critical surface may not exceed the threshold $\tau = f(\sigma)$.

- Stationary Stress Condition: $\dot{\sigma} = \boldsymbol{E}_t : \dot{\boldsymbol{\epsilon}} = 0 \iff \det(\boldsymbol{E}_t) = 0$.
  The stationary stress condition can be imagined as a stress-strain diagram that approaches a horizontal tangent at the limit point. As a result, the tangential material operator becomes singular, which is characterized by the critical eigenpair: $\lambda_{min}(\boldsymbol{E}_t) = 0$ and $\dot{\boldsymbol{\epsilon}}_{cr} = \dot{\boldsymbol{\epsilon}}_p$. The corresponding arguments of stationary second order work $d^2W = \dot{\boldsymbol{\epsilon}} : \boldsymbol{E}_t : \dot{\boldsymbol{\epsilon}}$, provide necessary, but not sufficient conditions for stationary stress values in the case of loss of symmetry of the material operator $\boldsymbol{E}_t \neq \boldsymbol{E}_t^t$ - for example in case of nonassociated plastic flow. The stationary stress condition is kinematically equivalent with the continuous failure concept.

- Localization Condition: $[\![\dot{t}]\!] = \boldsymbol{Q}_L \cdot \boldsymbol{M} = 0 \iff \det(\boldsymbol{Q}_L) = 0$.
  The localization condition detects the formation of spatial discontinuities along singularity surfaces defined by the vector $\boldsymbol{N}$. We speak about weak and strong discontinuities depending on the severity of jumps in the kinematic fields. In the localization case, the important aspect is the direction $\boldsymbol{N}$ of the normal to the discontinuity surface which is an implicit function of the localization tensor $\boldsymbol{Q}_L = \boldsymbol{N} \cdot \boldsymbol{E}_t \cdot \boldsymbol{N}$. Thus the eigenvalue $\eta_{min}(\boldsymbol{Q}_L) = 0$ and the corresponding eigenvector $\boldsymbol{M}$ determine the character of the failure mode. This holds for both weak as well as strong discontinuities which exhibit jumps in the strain $[\![\dot{\boldsymbol{\epsilon}}_L]\!] \propto \boldsymbol{M} \otimes \boldsymbol{N}$ or in the displacement field $[\![\dot{u}_L]\!] \propto \boldsymbol{M}$.

In what follows, the implications of these three failure concepts and the prediction of ensuing failure mode will be examined for pressure sensitive elastoplastic materials.

(a) Limit State Condition: This is a generalization of the traditional Mohr concept of strength which shows that the orientations of the critical slip planes remain fixed in the case of a straight failure envelope for dry friction according to Coulomb. In other terms. the Mohr-Coulomb envelope condition results in the same mixed failure mode irrespectively of the loading in tension, compression or shear. This shortcoming for cohesive materials led to a variety of proposals to augment the Mohr-Coulomb criterion by a tension cut-off criterion according to Rankine. A unifying formulation dates back to the curvilinear envelope proposal by LEON, [1935] who argued in favor of a parabolic shape of the Mohr envelope. Thereby, parameterization of the parabolic shape in terms of the uniaxial tensile and compressive strength values results in interesting limitations. In order to assure mode I failure in direct tension the uniaxial compressive strength must be at least three times its tensile strength. In the terminology of the concrete community this infers that $f'_c \geq 3 f'_t$. Moreover, when torsional loading in pure shear results in mode I failure, $\tau_s = f'_t$, then the uniaxial compressive strength must satisfy the inequality $f'_c \geq 2(1 + \sqrt{2}) f'_t$. With these constraints the parabolic Leon envelope captures the transition from mode I in direct tension and pure shear (torsion), to mixed mode failure under uniaxial compression. The direction of the critical failure planes varies between $0 \leq \theta_{cr} = \pi/4 - \phi/2 < \phi/4$, whereby the angle of friction ϕ corresponds to the slope of the parabolic envelope curve at the contact point of the stress circle, WILLAM AND IORDACHE, [1994B] (see Fig. 1).
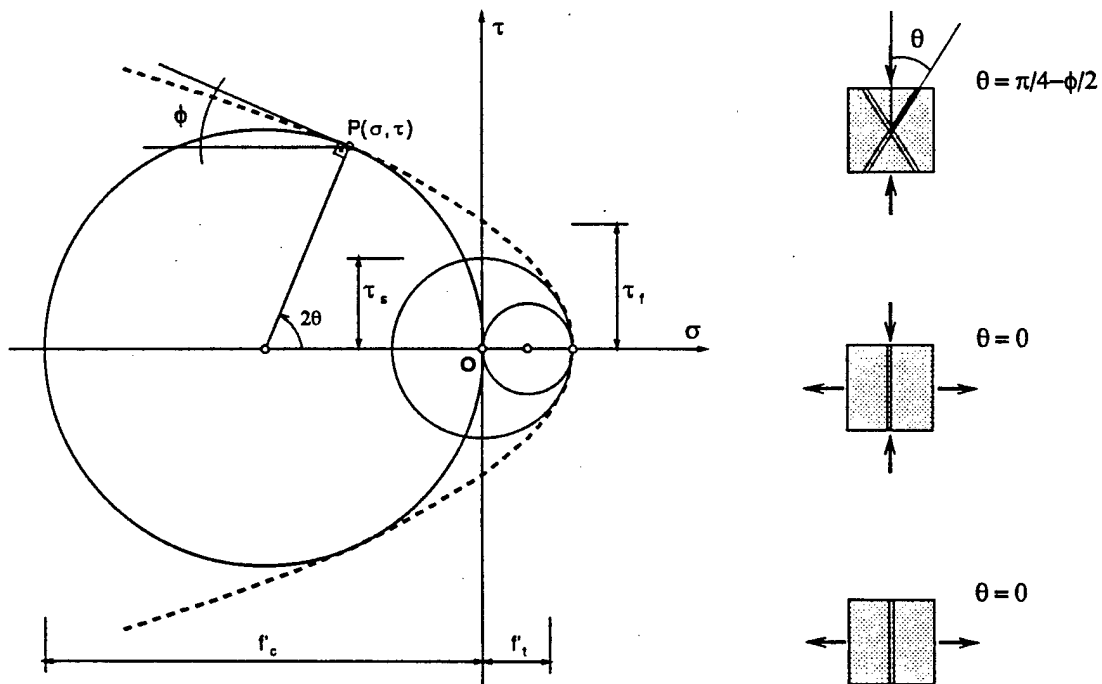
Figure 1: Variation of failure mode when the parabolic Mohr envelope (Leon criterion) is subjected to uniaxial compression, pure shear and uniaxial tension. The failure mode depends on the contact point location and varies with the state of stress ($f'_c = 2(1 + \sqrt{2})f'_t$).

(b) Stationary Stress Condition: When the stationary stress condition plots as a horizontal asymptote at the limit point of the stress-strain diagram, the tangent material law exhibits a singularity with the critical eigenpair $\lambda_{min}(\mathbf{E}_{tan}) = 0$ and $\dot{\epsilon} \rightarrow \dot{\epsilon}_{crit}$. In elastoplasticity and scalar damage CAROL ET AL, [1994], RIZZI ET AL [1995A] this singularity is normally governed by the directional properties of the evolution law $\dot{\epsilon}_{crit} \propto \mathbf{m}$, where the direction of the growth law is expressed in terms of the gradient of a potential function of stress. In short, stationary stress states are mobilized when the critical strain rate is normal to the loading surface. Figure 2 illustrates the response prediction of a Drucker-Prager elastic perfectly platic solid subjected to uniaxial compression. After reaching the yield limit in plane stress case, the state of stress becomes stationary, and satisfies:

$$\dot{\sigma} = \mathbf{E}_t : \dot{\epsilon}_{cr} = 0 \tag{1}$$

At this point, the tangent material operator becomes singular $\det(\mathbf{E}_t) = 0$, and the strain rate will be the eigenvector corresponding to the zero eigenvalue. Since we can also write the stress-strain relationship as:

$$\dot{\sigma} = \mathbf{E}_0 : (\dot{\epsilon}_{cr} - \dot{\epsilon}_p) = 0 \tag{2}$$

where $\mathbf{E}_0$ is the positive definite elastic material operator, the condition to reach a stationary value is:

$$\boxed{\text{Stationarity Condition: } \dot{\sigma} = 0 \quad \Leftrightarrow \quad \dot{\epsilon}_{cr} = \dot{\epsilon}_p} \tag{3}$$

In case of an associated flow rule, this implies that the critical strain rate becomes normal to the yield surface: $\dot{\epsilon}_{cr} = \dot{\lambda}\,\mathbf{n}$ and coincides with the direction of the plastic strain rate.

In plane strain we observe 'apparent hardening' due to the kinematic constraint which results in significant stress redistribution upon continued loading. The stresses still increase after the after the yield surface has been reached at the contact point, until the zero out-of-plane kinematic constraint results in zero out-of-plane plastic strain rates. When this stationarity condition is satisfied, the stresses reach a maximum point and a horizontal stress-strain response follows:

$$\left.\begin{array}{ll} \dot{\sigma} = \mathbf{E}_o : (\dot{\epsilon}_{cr} - \dot{\epsilon}_p) = 0 & \Leftrightarrow \quad \dot{\epsilon}_{cr} = \dot{\epsilon}_p \\ \text{Plane Strain constraint: } \epsilon_{33} = 0 & \Rightarrow \quad \dot{\epsilon}_{33} = 0 \\ \text{Flow Rule: } \dot{\epsilon}_p = \dot{\lambda}\,\mathbf{m} \;\; (\dot{\lambda} \neq 0) & \Rightarrow \quad \dot{\epsilon}^p_{33} = \dot{\lambda}\,m_{33} \end{array}\right\} \Rightarrow$$

$$\boxed{\text{Necessary Condition in Plane Strain for } \dot{\sigma} = 0 \;\; : \;\; m_{33} = 0} \tag{4}$$

This apparent hardening in axial compression would approach infinity if condition (4) cannot be satisfied. In other words, if $m_{33} \neq 0$ in plane strain conditions, the stress path increases without bound, even if it still satisfies the yield restraint. This happens in the uniaxial compression case when the Drucker-Prager yield function is calibrated for a strength ratio larger than 3:1 ($f'_c/f'_t \geq 3/1$, or $\alpha_1 \geq \sqrt{3}/6$). For this strength ratio the kinematic plane strain constraint eliminates the inherent singularity of the elastic perfectly plastic material law ($\dot{\sigma} = \mathbf{E}_t : \dot{\epsilon} \neq 0$) in the compression region, and the stress path can no longer reach a stationary value. Under stress control, the stationarity requirement results in the well-established argument that the elastoplastic tangent operator turns singular when the strain
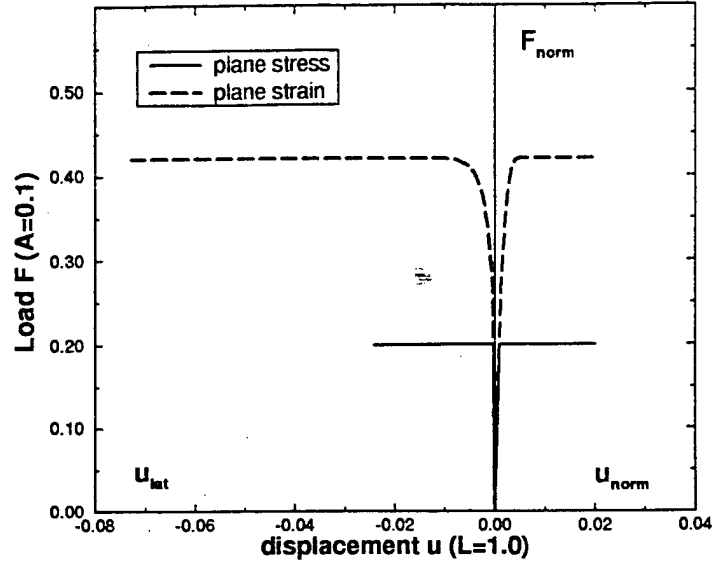
Figure 2: Apparent Hardening of plane strain versus plane stress when an elastic perfectly plastic Drucker-Prager solid ($f'_c/f'_t = 2/1$) is subjected to compression.

rate is coaxial with the plastic flow direction ($\dot{\epsilon} = \alpha \, m$) and the plastic hardening modulus diminishes to zero: $H_p \to 0$. In other terms, the regularization of positive hardening reduces to zero when the plastic modulus approaches zero. Under strain or mixed control the critical eigenmode of the tangent operator may be constrained and may suppress the underlying singularity (as long as the coaxiality requirement is not satisfied). Thus the zero hardening condition is a necessary but not a sufficient condition for reaching stationary stress values in the form of limit points.

On the other side, when the hardening modulus is negative ($H_p < 0$), after reaching the yield surface at the contact point, the apparent hardening due to the kinematic plane strain constraint is counteracted by softening. In the limit, the stationarity condition $\dot{\sigma} = 0$ will be satisfied at the contact point, at the transition point between the positive elastic loading and negative plastic softening. Equation (4) shows that at the limit point the zero condition of out-of-plane plastic strain increment $m_{33} = 0$ needs to be satisfied. Figure 3 summarizes the variation of the uniaxial compression stress versus the uniaxial strain for a Drucker-Prager material when two cases, perfectly plastic and linear softening behavior are considered. In plane strain, the apparent hardening, that appears in the perfectly plastic case, is reduced significantly due to softening, and as a result, the limit point of stationary stress is close to the contact point of initial yield.

(c) Localization Condition: The localization condition detects the formation of spatial discontinuities along singularity surfaces defined by the vector N. We speak of weak and strong discontinuities depending on the severity of jumps which emerge first in the strain rate and then in the velocity field. The important result of localization analysis is the direction N of the discontinuity surface which is an implicit function of the localization tensor
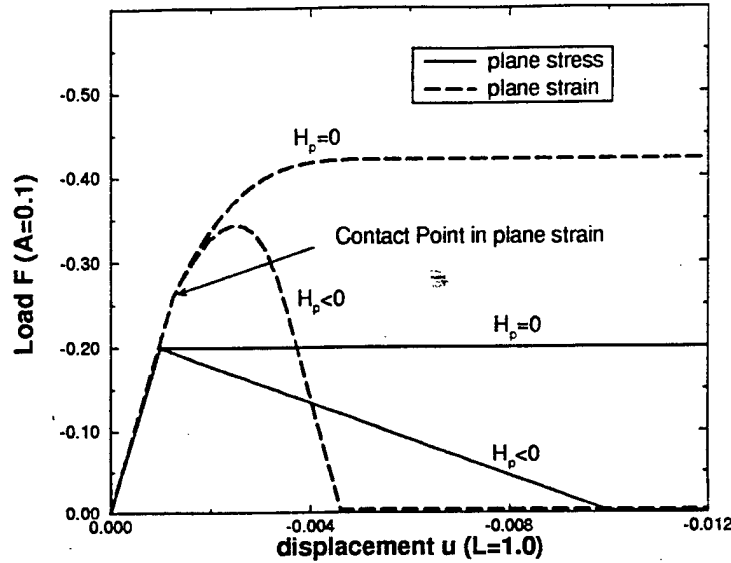
Figure 3: Compression response of elastic perfectly plastic and softening Drucker-Prager solid $(f'_c/f'_t = 2/1)$ in plane stress and in plane strain.

$Q_L = N \cdot E_t \cdot N$. Thus the eigenpair $\eta(Q_L) = 0$ and the corresponding eigenvector M determine the character of the failure mode. This holds for weak as well as for strong discontinuities which exhibit jumps in the strain rate $[\![\dot{\epsilon}_{loc}]\!] \propto (M \otimes N)$ and the velocity field $[\![u_{loc}]\!] \propto M$.

This localization condition may be phrased in terms of a critical hardening modulus H_p which is required for localization along the direction N.

$$\boxed{H_p + n : E_o : m = a \cdot Q_o^{-1} \cdot b} \tag{5}$$

$$a = n : E_o \cdot N , \quad b = N \cdot E_o : m \quad \text{and} \quad Q_o = N \cdot E_o \cdot N$$

The onset of localization arises when the critical hardening modulus reaches a maximum for all possible orientations N. This problem was solved analytically for non-associated elastoplasticity in OTTOSEN ET AL, [1992] with the help of Lagrange multipliers.

The results of the parabolic extension of the Drucker-Prager model are shown in figure 4 which demonstrates the effect of the parabolic yield surface on the failure mode. In fact, the localization diagram demonstrates the change of orientation of the critical discontinuity surface. The parabolic formulation results in mode I failure for loading in axial tension and in mixed mode failure for loading in pure shear and axial compression. It gradually approaches mode II failure with $N \perp M$ when the confinement increases and the hydrostatic-deviatoric interaction decouples.

Geometric Representation of the Localization Condition

An alternative geometric approach for discontinuous bifurcation analysis was recently proposed for continuum damage models in classical continua in BENALLAL AND COMI [1995] and
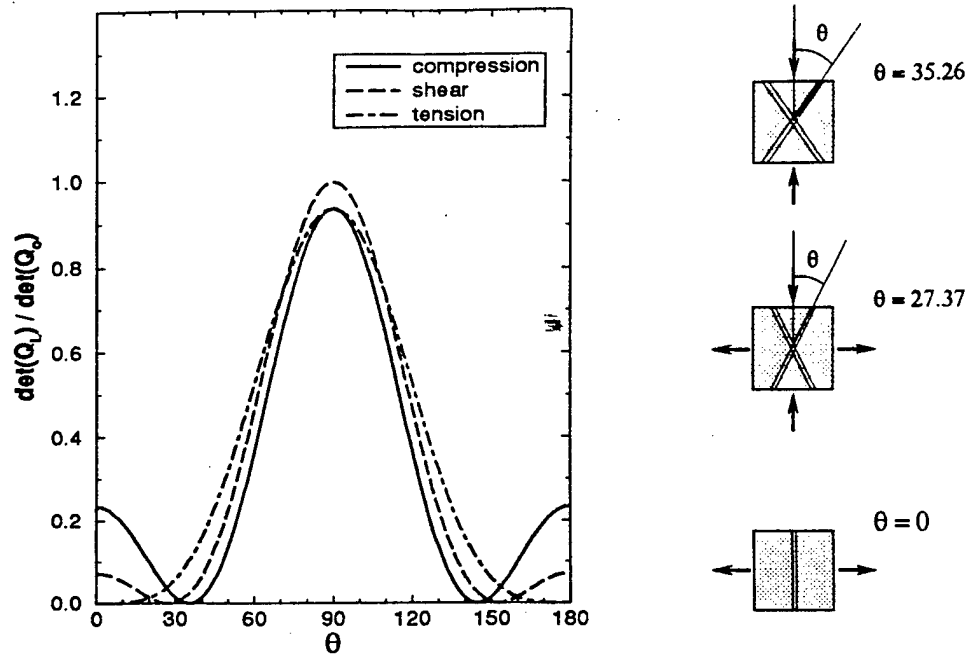
Figure 4: Localization properties of parabolic Drucker-Prager extension in plane strain

RIZZI ET AL [1995A]. There, the critical localization directions and the maximum hardening modulus were determined with the aid of the geometric representation of the stress/strain state in Mohr's space. Here, this geometric concept is used for discontinuous bifurcation analysis of Drucker-Prager-type elastoplastic materials.

The yield surface and the plastic potential function are for non-associated plastic flow :

$$F = \sqrt{J_2} + \alpha_1 \, I_1 - \beta_1 \quad \text{and} \quad Q = \sqrt{J_2} + \alpha_2 \, I_1 - \beta_2 \tag{6}$$

and their gradients with respect to the stress tensor

$$n = \frac{\partial F}{\partial \sigma} = \frac{1}{2 \sqrt{J_2}} \, s + \alpha_1 \, I_1 \quad \text{and} \quad m = \frac{\partial Q}{\partial \sigma} = \frac{1}{2 \sqrt{J_2}} \, s + \alpha_2 \, I_1 \tag{7}$$

In the three dimensional case, the elastic material operator E_o, the acoustic tensor Q_o and it's inverse are, in index notation:

$$
\begin{aligned}
E^o_{ijkl} &= \frac{E}{1+\nu} \left[\frac{\nu}{1-2\,\nu} \, \delta_{ij}\delta_{kl} + \frac{1}{2} \left(\delta_{ik}\delta_{jl} + \delta_{il}\delta_{jk} \right) \right] \\
Q^o_{jk} &= N_i \, E^o_{ijkl} \, N_l = \frac{E}{2\,(1+\nu)} \left(\delta_{jk} + \frac{1}{1-2\,\nu} \, N_j \, N_k \right) \\
Q^{-1}_{jk} &= \frac{2\,(1+\nu)}{E} \left(\delta_{jk} - \frac{1}{2\,(1-\nu)} \, N_j \, N_k \right)
\end{aligned}
\tag{8}
$$

The normal and shear components on a plane defined by the normal vector N is in our notation:

$$\sigma = N \cdot \sigma \cdot N \, , \quad s = N \cdot s \cdot N$$

$$\tau^2 = (\boldsymbol{N} \cdot \boldsymbol{\sigma}) \cdot (\boldsymbol{N} \cdot \boldsymbol{\sigma}) - (\boldsymbol{N} \cdot \boldsymbol{\sigma} \cdot \boldsymbol{N})^2 = (\boldsymbol{N} \cdot \boldsymbol{s}) \cdot (\boldsymbol{N} \cdot \boldsymbol{s}) - (\boldsymbol{N} \cdot \boldsymbol{s} \cdot \boldsymbol{N})^2$$

$$\overline{\sigma} = \frac{\sigma}{\sqrt{J_2}} , \qquad \overline{s} = \frac{s}{\sqrt{J_2}} , \qquad \overline{\tau} = \frac{\tau}{\sqrt{J_2}} \tag{9}$$

The so-called traction vectors $\boldsymbol{a}$ and $\boldsymbol{b}$ of localization analysis have the format:

$$a_j \;\; = \;\; N_i \, E^o_{ijkl} \, m_{kl} = \alpha_2 \, \frac{E}{1 - 2\,\nu} \, N_j + \frac{E}{2\,(1+\nu)} \, N_i \, \overline{s_{ij}}$$

$$b_k \;\; = \;\; n_{ij} \, E^o_{ijkl} \, N_l = \alpha_1 \, \frac{E}{1 - 2\,\nu} \, N_k + \frac{E}{2\,(1+\nu)} \, N_l \, \overline{s_{lk}} \tag{10}$$

As a result, the analytical localization condition may be written as:

$$H_p + \boldsymbol{n} : \boldsymbol{E}_o : \boldsymbol{m} \;\; = \;\; H_p + E \left[\frac{3\,\alpha_1\,\alpha_2}{1 - 2\,\nu} + \frac{1}{2\,(1+\nu)} \right] \tag{11}$$

$$\boldsymbol{b} \cdot \boldsymbol{Q}_o^{-1} \cdot \boldsymbol{a} \;\; = \;\; \frac{E}{2\,(1+\nu)} \, \overline{\tau}^2 + E \, \frac{(1+\nu)(1 - 2\,\nu)}{1 - \nu} \left[\frac{1}{4\,(1+\nu)^2} \, \overline{s}^2 \right.$$

$$+ \;\; \left. \frac{\alpha_1 + \alpha_2}{2\,(1+\nu)(1 - 2\,\nu)} \, \overline{s} + \frac{\alpha_1 \, \alpha_2}{(1 - 2\,\nu)^2} \right] \tag{12}$$

and the localization ellipse reads in Mohr stress coordinates:

$$\boxed{ \frac{(\overline{\sigma} - \overline{\sigma}_o)^2}{A^2} + \frac{\overline{\tau}^2}{B^2} = 1 } \tag{13}$$

with

$$\overline{\sigma}_o \;\; = \;\; \frac{1}{3} \, \overline{I}_1 - \frac{1+\nu}{1 - 2\,\nu} \, (\alpha_1 + \alpha_2)$$

$$B^2 \;\; = \;\; \frac{2\,(1+\nu)}{E} \, H_p + 1 + \alpha_1 \, \alpha_2 \, \frac{6\,(1+\nu)}{1 - 2\,\nu} + (\alpha_1 - \alpha_2)^2 \, \frac{(1+\nu)^2}{2\,(1-\nu)(1 - 2\,\nu)}$$

$$A^2 \;\; = \;\; \frac{2\,(1-\nu)}{1 - 2\,\nu} \, B^2 \tag{14}$$

For $\overline{\tau} \leq A$, $\overline{\tau} \leq B$, and $|\overline{\sigma}_c - \overline{\sigma}_o| \leq A - \overline{\tau}$, tangency may be enforced between the ellipse and the Mohr's Circle of stress

$$\boxed{ (\overline{\sigma} - \overline{\sigma}_c)^2 + \overline{\tau}^2 = \overline{r}^2 } \tag{15}$$

when the critical failure angle θ_{cr}, and the critical hardening parameter H_{cr} are reached according to the geometric conditions shown in figure 5:

$$H_{cr} \;\; = \;\; \frac{E}{2\,(1+\nu)} \left\{ \frac{r}{\sqrt{J_2}} + (1 - 2\,\nu) \left[\frac{\sigma_c}{\sqrt{J_2}} - \frac{I_1}{3\,\sqrt{J_2}} + \frac{1+\nu}{1 - 2\,\nu} \, (\alpha_1 + \alpha_2) \right]^2 \right.$$

$$- \;\; \left. 1 - \alpha_1 \, \alpha_2 \, \frac{6\,(1+\nu)}{1 - 2\,\nu} - (\alpha_1 - \alpha_2)^2 \, \frac{(1+\nu)^2}{2\,(1-\nu)(1 - 2\,\nu)} \right\} \tag{16}$$
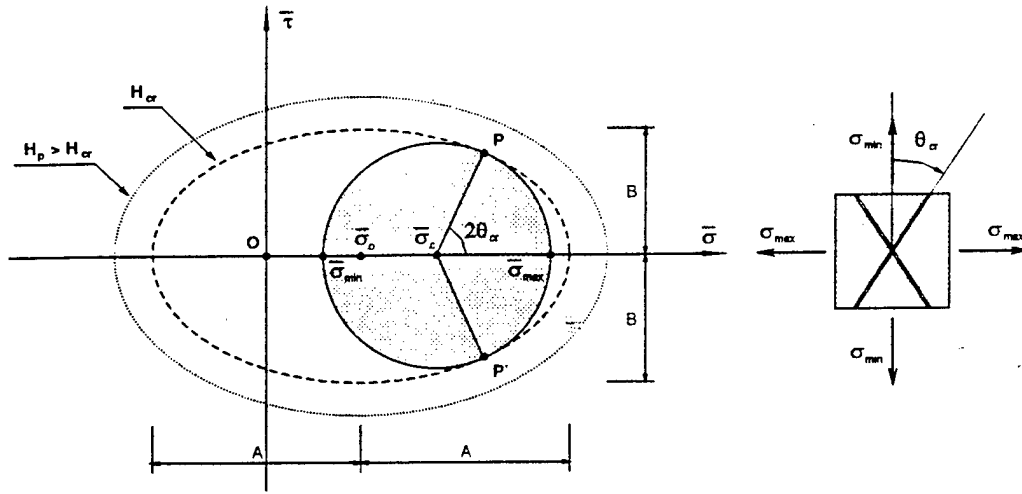
Figure 5: Tangency of the Localization Ellipse and Mohr's Circle establish the localized failure mode in terms of the angle θ_{cr} between the minor principal stress direction (σ_{min}) and the failure plane

$$\tan^2(\theta) = \frac{r - \left|\left(\sigma_c - \frac{1}{3}I_1\right)(1 - 2\nu) + \sqrt{J_2}\,(\alpha_1 + \alpha_2)(1 + \nu)\right|}{r + \left|\left(\sigma_c - \frac{1}{3}I_1\right)(1 - 2\nu) + \sqrt{J_2}\,(\alpha_1 + \alpha_2)(1 + \nu)\right|}$$

$$\theta_{cr} = \begin{cases} \theta & \text{if } \sigma_c \geq \sigma_o \\ \frac{\pi}{2} - \theta & \text{if } \sigma_c < \sigma_o \end{cases} \tag{17}$$

From equation 16 it can be seen that the hardening parameter's value does not influence the critical localization angle. The variation of H_p changes only the size of the ellipse, but it's center and the ratio of half axes (A/B) do not change (14). In contrast, Poisson's ratio does affect the shape and position of the ellipse, consequently it influences the localization angle. It can be observed that for a Poisson's ratio $\nu \to 0.5$, if $\alpha_1 = \alpha_2 = 0$, the localization ellipse degenerates into two straight lines, parallel with σ-axis. As a result, the angle of localized failure for von Mises elastoplasticity is $\theta_{cr} \to 45^o$ with respect to the minor principal stress direction (σ_{min}) for all loading cases.

Failure in the Large

The effects of localization and confinement on the failure behavior are best understood with some elementary examples. To this end we examine the model problem of a Drucker-Prager material which exhibits a very slight amount of softening of the cohesive strength. From the previous analysis we know that dimensional reductions of plane stress and plane strain lead to discontinuous bifurcation for zero hardening $H_{cr} = 0$, in plane strain however only after the stationary point $\dot{\sigma} = 0$ has been reached. The elliptic localization envelopes in Fig. 6 illustrate failure in the small in terms of the directional properties of discontinuities which differ in orientation when failure in plane stress is compared with that in plane strain.
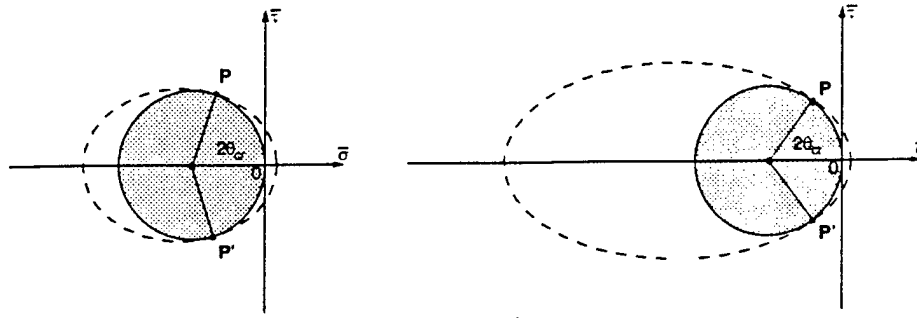
Figure 6: Different Failure Modes of elastic perfectly plastic Drucker-Prager material in compression for plane stress (left $\theta^s_{cr} = 41.81°$) and plane strain (right $\theta^e_{cr} = 26.12°$). In plane strain the localization condition for perfect plasticity is reached only at the stationary point

For failure in the large let us consider a square domain which is discretized with a random mesh of constant strain triangles with homogeneous material properties in case (a), and with heterogeneous properties in case (b) corresponding to a two phase particle composite, with elastic inclusions which are considerably stiffer than the elastoplastic matrix material (see Fig. 7).
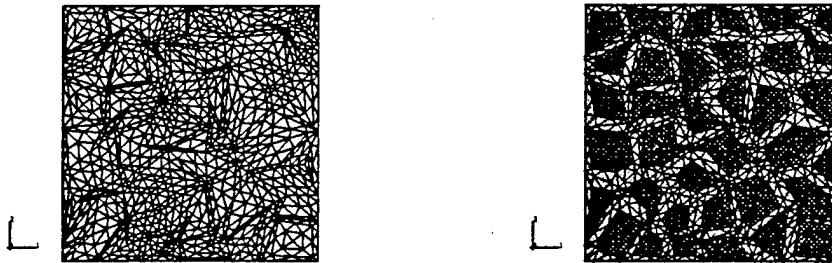
Figure 7: Drucker-Prager Failure Analysis of Compression Problem - homogeneous vs. two-phase matrix-aggregate composite, $E_m = 2000\,ksi$, contrast ratio $E_a/E_m = 5/1$, $\nu_a = \nu_m = 0.2$, $f'_c = 2\,ksi$, $f'_t = 1\,ksi$

Uniaxial compression leads to the localized failure modes depicted in Fig. 8 which compares the plastic strain distribution for plane stress and plane strain triggered by a small imperfection in the form of a weak element in the center of the solution domain . In both cases of plane stress and plane strain, the orientations of concentrated inelastic deformations reproduce the directional properties of localization analysis in Fig. 6.

The load-deformation response results in Fig. 9 show the apparent hardening in plane strain when compared to plane stress. The kinematic out-of-plane constraints retards the stress path to reach the stationary point. The results of the discretized finite element solutions solving an IBVP show close agreement with the constitutive predictions during continuous failure. Only at a fairly advanced stage of the post-peak response the two solutions diverge
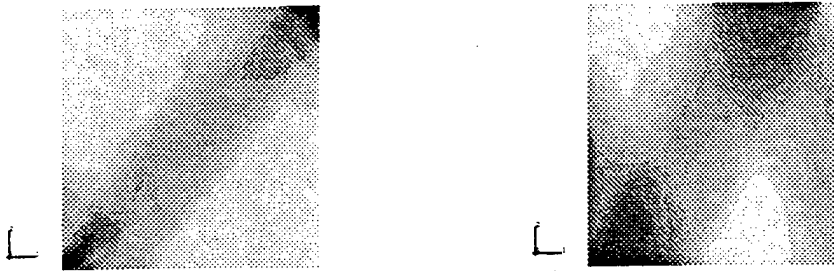
Figure 8: Drucker-Prager Compression Problem: formation of localized failure mode in plane stress (left $\theta_{cr}^e = 41.81^o$), and plane strain (right $\theta_{cr}^e = 26.12^o$)
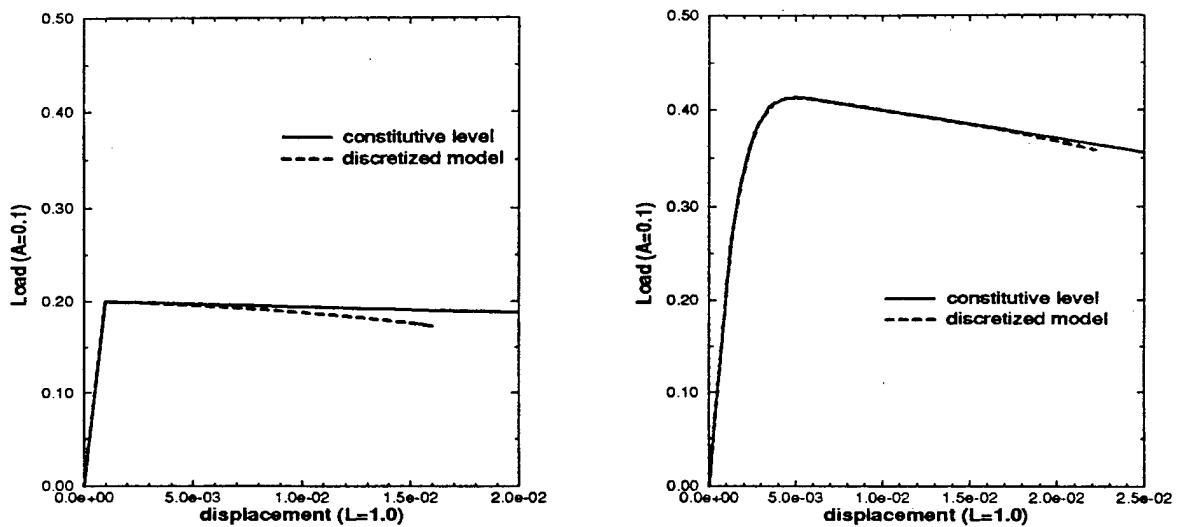

Figure 9: Drucker-Prager Compression Problem: stress-strain response at the material level and at the structural level, in plane stress (left), and plane strain (right)

due to sudden localization which results in loss of convergence of the finite element solution in the softening regime in spite of arc-length control of the Rix-Wempner type.

The different failure modes of the composite studies are depicted in figure 10. The two-phase matrix-aggregate composite introduces additional stress raisers due to mismatch of the constituents. In plane stress the elastic aggregate increases the strength of the composite beyond that of the matrix, but it decreases the overall ductility when compared to that of the homogeneous material problem, see figure 9. The deterioration of ductility in plane stress is in direct contrast to the hardening behavior in plane strain. Moreover, the distribution of plastic strain shows that the localized failure mode in plane stress is oriented at the same angle as the localization direction of the Drucker-Prager matrix material in figure 8 in spite of the presence of elastic aggregate particles. In contrast, in plane strain the two-phase particle composite exhibits distributed plastic flow throughout the matrix which is the main reason for the hardening response at the composite level. In fact, the composite response in

plane strain does not even reach failure in the form of limit point behavior. The kinematic constraint dramatically raises the overall strength and ductility of the composite in spite of the additional stress raisers due to mismatch of the constituents. Hence. we can expect that the actual three-dimensional failure behavior of particle composites will lie somewhere between the two limiting assumptions of plane stress and plane strain.

In sum. the failure of the particle composite is governed by the weakest constituent. in this case the Drucker-Prager matrix, while the stiffness and strength properties are increased by the elastic aggregate particles. The ductility however is markedly affected by the confinement when the plane stress response is compared to the plane stain results. In the former case strain localization decreases ductility in the attempt to drive a failure path of minimal resistance through the solution domain. In the latter case, apparent hardening prevails and prevents altogether failure to occur.
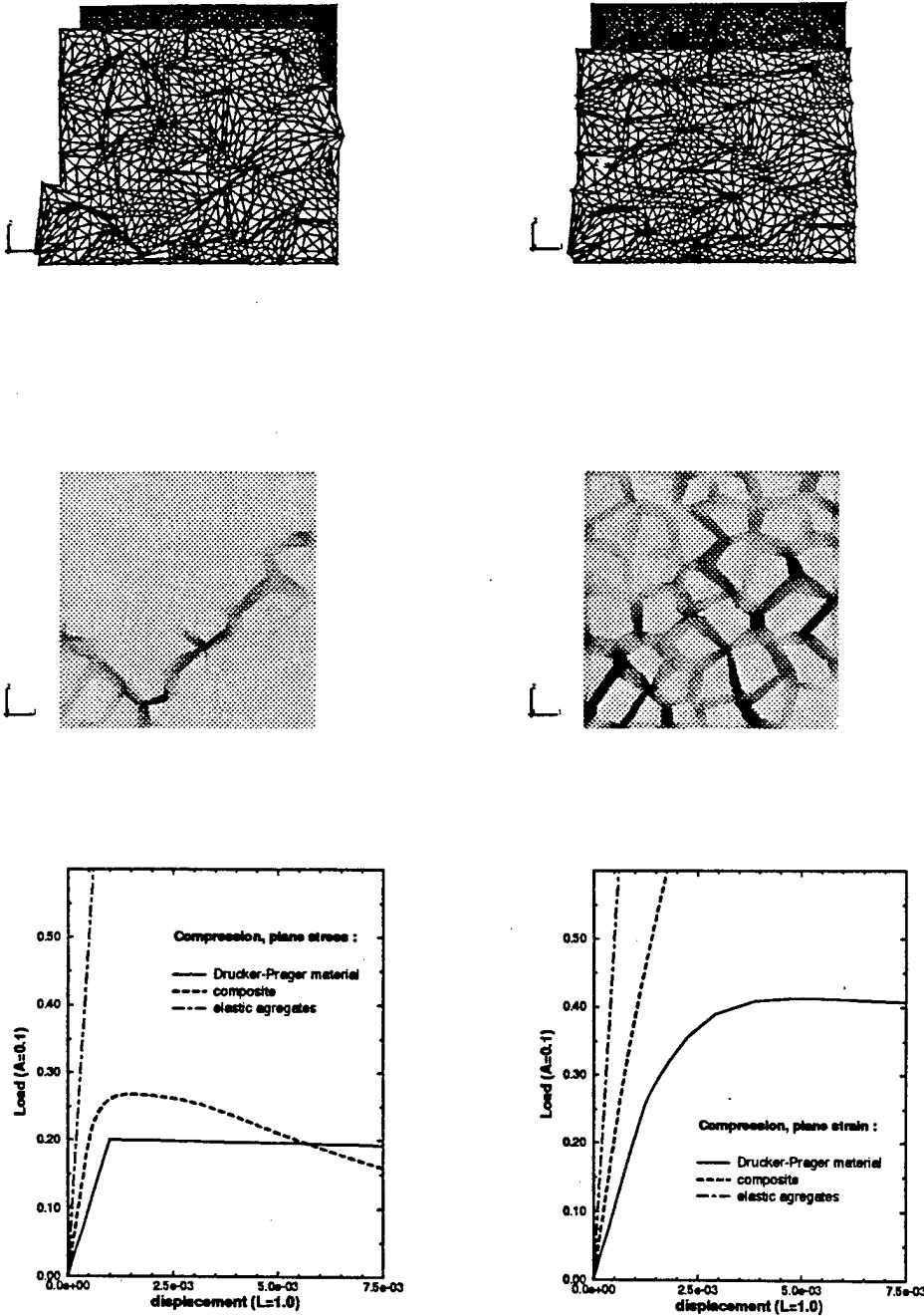
Figure 10: Drucker-Prager two-phase composite compression problem: Plane Stress (left), versus Plane Strain (right) response.

List of Publications

1. Carol, I., Rizzi, E. and K. Willam, (1994), "A Unified Theory of Elastic Degradation and Damage Based on a Loading Surface", Int. J. Solids and Structures. 31(20), pp. 2835-2865.

2. Benallal, A. and C. Comi, (1995), "Localisation Analysis via a Geometrical Method". to appear in in IJSS, Vol. 32.

3. Dietsche, A. and K. Willam, (1995), "Boundary Effects in Elastoplastic Cosserat Continua", accepted for publ. in IJSS, Vol. 32.

4. Etse, G. and K. Willam, (1994), "A Fracture Energy-Based Constitutive Formulation for Inelastic Behavior of Plain Concrete", ASCE J. Eng. Mechanics, 120 (9), pp. 1983-2011.

5. Guzina, B.B., Rizzi, E., Willam, K. and R.Y.S. Pak , (1995), "Failure Detection of Smeared Crack Formulations", ASCE J. Eng. Mechanics, Vol. 121, pp. 150-161.

6. Iordache, M.-M. , (1995), "A Comparative Study of Failure in Classical and Micropolar Elasto-plasticity", Ph.D. thesis, CEAE Department, University of Colorado, Boulder.

7. Lee, Y.-H. and K. Willam, (1995), "Mechanical Properties of Concrete in Uniaxial Compression", submitted for publication in ACI-Structures Journal.

8. Lee, Y.-H. and K. Willam, (1995), "Anisotropic Vertex Plasticity Formulation of Concrete in Plane Stress", submitted for publication in ASCE J. Eng Mechs, 1995.

9. Leon, A.,(1935), "Über die Scherfestigkeit des Betons", Beton und Eisen, 34, pp 130-135.

10. Ottosen, N. S., and Runesson, K., (1991), "Properties of Discontinuous Bifurcation Solutions in Elastoplasticity", Int. J. Solids and Structures, Vol. 27 (4), pp 401-421.

11. Radakovic, Z., Bond, L. and K. Willam, (1995), "Ultrasonic Detection of Plastic Yielding in Steel Specimens", Proc. Annual Review of Progress in Quantitative NDE, Plenum Press, New York, pp. 1593-1600.

12. Rizzi, E., Carol, I. and K. Willam, (1995a), "Localization Analysis of Elastic Degradation with Application to Scalar Damage", ASCE J. Eng. Mechanics, Vol. 121, pp. 541-554.

13. Rizzi, E., Maier, G. and Willam, K., (1995b), "On Failure Indicators in Multi-Dissipative Materials", accepted for publ. in IJSS, Vol. 32.

14. Steinmann, P. and K. Willam, (1994), "Finite Element Analysis of Spatial Discontinuities due to Elastoplastic Bifurcation", ASCE J. Eng. Mechanics, Vol. 120, pp. 2428-2442.

15. Willam, K., Münz, T., Etse, G. and Menétrey, Ph., (1994a), "Failure Conditions and Localization in Concrete", Proc. Euro-C Conf, Eds. H. Mang, N. Bicanic, R. deBorst, Pineridge Press Swansea, pp 263-282.

16. Willam, K. and Iordache, M.-M., (1994b), "Fundamental Aspects of Failure Modes in Brittle Solids", Euro-US Workshop on Fracture and Damage in Quasibrittle Materials, Prague, Sept. 20-23, 1994, pp. 35-67.

17. Willam, K. and Iordache, M.-M., (1994c), "Failure Modes in Quasibrittle Materials", AFOSR-Contractors Meeting, Sept. 1994, University of Illinois, Chicago.

18. Willam, K., Dietsche, A., Iordache, M.-M. and Steinmann, P., (1995a), "Localization in Micropolar Continua", Chapter 9 in Cont. Models for Materials with Microstructure, H-B. Mühlhaus Ed., Wiley Intl. Chichester, UK.

19. Willam, K. and Iordache, M.-M., (1995b), "Failure Modes in Cohesive-Frictional Materials", submitted for publ. in Intl. J. of Cohesive-Frictional Materials, Wiley Interscience, UK.